AMERICAN SOCIETY FOR MICROBIOLOGY | Journal of Virology®

VACCINES AND ANTIVIRAL AGENTS

High-Throughput Protein Engineering Improves the Antigenicity and Stability of Soluble HIV-1 Envelope Glycoprotein SOSIP Trimers

Jonathan T. Sullivan,[a] Chidananda Sulli,[a] Alberto Nilo,[b] Anila Yasmeen,[b] Gabriel Ozorowski,[c] Rogier W. Sanders,[b,d] Andrew B. Ward,[c] P. J. Klasse,[b] John P. Moore,[b] Benjamin J. Doranz[a]

Integral Molecular, Philadelphia, Pennsylvania, USA[a]; Department of Microbiology and Immunology, Weill Medical College of Cornell University, New York, New York, USA[b]; Department of Integrative Structural and Computational Biology, Center for HIV/AIDS Vaccine Immunology and Immunogen Discovery, International AIDS Vaccine Initiative Neutralizing Antibody Center, and Collaboration for AIDS Vaccine Discovery, The Scripps Research Institute, La Jolla, California, USA[c]; Department of Medical Microbiology, Academic Medical Center, University of Amsterdam, Amsterdam, The Netherlands[d]

ABSTRACT Soluble envelope glycoprotein (Env) trimers (SOSIP.664 gp140) are attractive HIV-1 vaccine candidates, with structures that mimic the native membrane-bound Env spike (gp160). Since engineering trimers can be limited by the difficulty of rationally predicting beneficial mutations, here we used a more comprehensive mutagenesis approach with the goal of identifying trimer variants with improved antigenic and stability properties. We created 341 cysteine pairs at predicted points of stabilization throughout gp140, 149 proline residue substitutions at every residue of the gp41 ectodomain, and 362 space-filling residue substitutions at every hydrophobic and aromatic residue in gp140. The parental protein target, the clade B strain B41 SOSIP.664 gp140, does not bind the broadly neutralizing antibody PGT151 and so was used here to identify improved variants that also provide insight into the structural basis for Env antigenicity. Each of the 852 mutants was expressed in human cells and screened for antigenicity using four different monoclonal antibodies (MAbs), including PGT151. We identified 29 trimer variants with antigenic improvements derived from each of the three mutagenesis strategies. We selected four variants (Q203F, T538F, I548F, and M629P) for more comprehensive biochemical, structural, and antigenicity analyses. The T538F substitution had the most beneficial effect overall, including restoration of the PGT151 epitope. The improved B41 SOSIP.664 trimer variants identified here may be useful for vaccine and structural studies.

IMPORTANCE Soluble Env trimers have become attractive HIV-1 vaccine candidates, but the prototype designs are capable of further improvement through protein engineering. Using a high-throughput screening technology (shotgun mutagenesis) to create and evaluate 852 variants, we were able to identify sequence changes that were beneficial to the antigenicity and stability of soluble trimers based on the clade B B41 *env* gene. The strategies described here may be useful for identifying a wider range of antigenically and structurally improved soluble trimers based on multiple genotypes for use in programs intended to create a broadly protective HIV-1 vaccine.

KEYWORDS gp140, human immunodeficiency virus, immunization, protein engineering, shotgun mutagenesis, trimer

Received 25 May 2017 **Accepted** 23 August 2017

Accepted manuscript posted online 6 September 2017

Citation Sullivan JT, Sulli C, Nilo A, Yasmeen A, Ozorowski G, Sanders RW, Ward AB, Klasse PJ, Moore JP, Doranz BJ. 2017. High-throughput protein engineering improves the antigenicity and stability of soluble HIV-1 envelope glycoprotein SOSIP trimers. J Virol 91:e00862-17. https://doi.org/10.1128/JVI.00862-17.

Editor Adolfo García-Sastre, Icahn School of Medicine at Mount Sinai

Address correspondence to John P. Moore, jpm2003@med.cornell.edu, or Benjamin J. Doranz, bdoranz@integralmolecular.com.

Soluble envelope glycoprotein (Env) trimers that mimic the native spikes on the HIV-1 surface are being developed as vaccines intended to induce broadly neutralizing antibodies (bNAbs) (reviewed in references 1 and 2). The design of the first generation of fully native-like trimers is designated SOSIP.664, reflecting the stabilization procedures that were used to produce a stable protein that could be successfully purified. Specifically, a SOSIP.664 gp140 trimer is proteolytically cleaved to separate the gp120 and gp41 subunits, has those two subunits covalently linked by an engineered intermolecular disulfide bond (A501C-T605C), contains a point substitution (I559P) within gp41 to maintain the trimer in its prefusion conformation, and is truncated at residue 664 to create a nonaggregating gp41 ectodomain ($gp41_{ECTO}$) structure (3). The total molecular size of the molecule is approximately 140 kDa (hence it is termed a gp140). For multiple genotypes, purification using broadly neutralizing antibody (bNAb) affinity columns results in nearly 100% native-like SOSIP.664 trimers (2).

SOSIP.664 trimers based on a number of different genotypes have now been produced and characterized (4–7). The prototype is the clade A trimer BG505 SOSIP.664, which is the basis of increasingly high-resolution structures (7–11) and which has induced autologous neutralizing MAbs against neutralization-resistant (classified as tier-2) viruses in animal experiments (12–14). Several other SOSIP.664 trimers have since been shown to have desirable antigenicity and immunogenicity properties (1, 12–14). A substantial body of antigenicity, structural, and immunogenicity data underpins why native-like trimers are now the basis of multiple vaccine design programs. However, the prototypic SOSIP.664 trimer design is clearly capable of improvement. Among the goals of such approaches are to increase the thermal stability of trimers and improve their ability to display bNAb epitopes while reducing their presentation of epitopes for nonneutralizing antibodies (non-NAbs). Two such trimer redesigns are each based on the use of high-resolution structural information to rationally engineer the trimer architecture (10, 12, 15–17). The "DS" variant of BG505 SOSIP.664 contains an engineered intra-gp120 disulfide bond linking residues 201 and 433 (10), while SOSIP.v4 trimers of several genotypes contain point substitutions within the C1 and V3 regions of gp120 (12).

The B41 clade B genotype of SOSIP.664 trimers offers additional opportunities for improvement through protein engineering. Like the BG505 prototype, B41 trimers are fully native-like when imaged by negative-stain electron microscopy after purification using the 2G12 bNAb, they display multiple epitopes for bNAbs but few for non-NAbs, and they induce strong autologous tier-2 bNAb responses (6, 14). However, the B41 trimers have a thermal denaturation midpoint (T_m) that is ~10°C lower than that of BG505 (~58°C versus ~68°C), and the interactions between the gp120 variable loops at the trimer apex are more flexible, as judged by electron microscopy (EM) (6). In EM images, the BG505 SOSIP.664 trimer is seen to be a completely homogeneous population of tri-lobed, propeller-like structures, with the trimer apex fully closed (7). Under similar conditions, B41 SOSIP.664 trimers are also completely native-like, but two subpopulations are visible in approximately equimolar proportions: the first is morphologically indistinguishable from the BG505 trimer, while the second is typified by satellite densities around the trimer apex that are ascribed to either the entire gp120 domain or the gp120 variable loops (6). The two classes likely represent snapshots of different positions in an equilibrium in which the trimers reversibly flicker between the fully closed and a partially open conformation. The same two subpopulations are also seen when trimers of several other genotypes are imaged (5, 12, 18). The partially open form is likely not the same as the more recently described, fully open conformation that mimics the CD4 receptor-bound state (19). It is also notable that B41 SOSIP.664 trimers do not bind the PGT151 bNAb, which recognizes a trimer-specific quaternary epitope at the gp120-gp41 interface on the corresponding virus (6). This observation implies that the gp120-gp41 interface of the soluble B41 trimer is capable of improvement.

Here, we employed a systematic approach to trimer engineering using both informed (rational) design and empirical (high-throughput) screening elements. By applying the most successful mutagenesis strategies for stabilizing HIV-1 trimers, but in a

high-throughput manner, we introduced (i) 341 different cysteine pairs at predicted points of stabilization throughout gp140 to create disulfide bonds that could "lock" protein regions to each other, (ii) 149 proline residue substitutions at every residue of $gp41_{ECTO}$ to stabilize desired conformations (or destabilize undesired conformations), and (iii) 362 space-filling residue substitutions at every hydrophobic and aromatic residue in gp140 to fill hydrophobic cavities within the trimer interior. These strategies resulted in 852 sequence-confirmed B41 SOSIP.664 mutants. After expressing each mutant in human HEK-293 cells and testing the resulting gp140 molecules for expression and antigenicity using various MAbs, we identified 29 variants with improved antigenic properties. Four variants (Q203F, T538F, I548F, and M629P) were tested using a wider variety of antigenic probes and biophysical techniques. All four constructs produced fully native-like trimers with improved antigenicity, and the T538F and I548F variants were also more thermostable. The T538F mutant was the most improved from the antigenicity and thermostability perspectives, including a restored PGT151 epitope.

RESULTS

Antigenic differences between B41 soluble SOSIP.664 gp140 and membrane-associated gp160. Our earlier studies demonstrated that bNAb PGT151 does not bind B41 SOSIP.664 trimers, despite the fact that PGT151 neutralizes the B41 virus (6). In this regard, B41 differs from BG505, as the latter trimer binds PGT151 and the virus is neutralized by it (6, 7). However, the B41 trimer binds multiple other bNAbs, implying that its lack of the PGT151 epitope arises from local and not general structural defects (6).

We studied the PGT151 binding versus neutralization discordance in more detail, in part to understand why the epitope was not displayed on the B41 trimer but also to identify variants with improved antigenicity. We first used three bNAbs, PGT151, PGT145, and PG9, as probes to detect both the expression and conformational integrity of Env trimers. These antibodies bind conformationally sensitive epitopes that are either dependent on (PGT151 and PGT145) or influenced by (PG9) the formation of a structurally intact trimer (5, 20, 21). PGT151 binds at the interface between gp120 and gp41, whereas PGT145 and PG9 recognize the trimer apex (Fig. 1A). We used flow cytometry and enzyme-linked immunosorbent assay (ELISA) methods to quantify bNAb binding to BG505 and B41 Env proteins. For both genotypes, gp160 proteins present on the surface of Env-transfected cells bound PGT151 strongly (Fig. 1B). In contrast, only the BG505 soluble SOSIP.664 trimer bound PGT151 in a capture ELISA (Fig. 1C). The absence of the PGT151 epitope from the soluble B41 trimer does not reflect a global structural defect, in that the trimer apex epitopes for the PG9 and PGT145 bNAbs were still present (Fig. 1D). PGT151, PG9, and PGT145 also all efficiently neutralized infection by B41-pseudotyped reporter viruses (Fig. 1E), although the lower slope of the neutralization curve for PGT151 suggests that even gp160 on the surface of the virus may exist in some conformations that are not readily accessible to PGT151.

Taken together, the ability of PGT151 to bind strongly to B41 trimers on the cell surface and to neutralize infection by the B41 virus supports our conclusion that the PGT151 epitope is compromised when this Env genotype is expressed in the form of a soluble SOSIP.664 gp140 trimer.

High-throughput engineering to identify improved B41 SOSIP.664 variants. As the gp120-gp41 interface region is a determinant of native-like trimers, we sought to identify variant B41 SOSIP.664 trimers that are more conformationally similar to membrane-associated gp160, as judged by the restoration of the PGT151 epitope. Use of the B41 strain of HIV-1 for these studies offers the opportunity to identify improved variants that also provide insight into the structural basis for Env antigenicity. By using a high-throughput mutagenesis strategy, three different categories of mutations were introduced into B41 SOSIP.664 gp140: (i) cysteine pairs with the goal of forming disulfide bonds to "lock" different protein regions to each other, (ii) proline residues to cause local conformational changes that stabilize desired conformations (or destabilize undesired conformations), and (iii) larger amino acids to fill hydrophobic cavities within

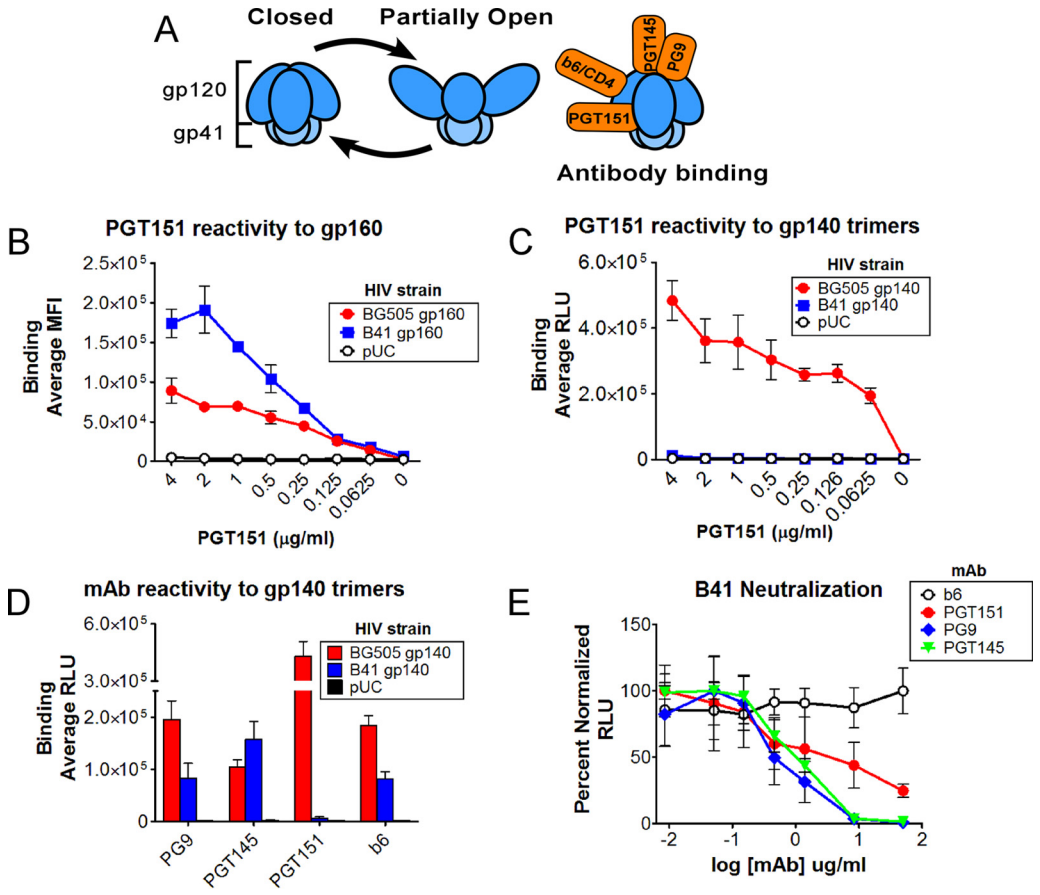

FIG 1 Antigenic differences between B41 soluble SOSIP.664 gp140 and membrane-associated gp160 trimers. (A) Cartoon showing closed versus partially open conformations of B41 gp140 and the general binding location of the key MAbs used in this study. (B) The quaternary structure-dependent bNAb PGT151 binds BG505 and B41 gp160 in a cell-based flow cytometry assay (pUC indicates a negative-control plasmid expressing no Env). (C) PGT151 binds BG505 but not B41 SOSIP.664 gp140 in an ELISA. (D) ELISA reactivity of BG505 and B41 SOSIP.664 gp140 with PG9 (1 μg/ml), PGT145 (0.5 μg/ml), PGT151 (2 μg/ml), and b6 (0.5 μg/ml). (E) B41 Env-pseudotyped reporter viruses are neutralized by PGT151, PG9, and PGT145 but not b6.

the trimer interior and thereby stabilize desired conformations by creating a greater bonding network. Each of these mutagenesis approaches has proven successful in engineering HIV-1 trimers previously but has been applied primarily to selected areas of the protein.

For dicysteine scanning mutagenesis, 38 residues in gp41 were identified as targets based on their proximity to gp120 and other elements of gp41 in the trimer structure. For each of the 38 residues, approximately 5 to 20 proximal residues were also individually mutated to cysteines to serve as potential disulfide bond partners (341 dicysteine mutants were made in total). The proline mutagenesis strategy was applied to every residue within the $gp41_{ECTO}$ component of the B41 SOSIP.664 construct (149 mutants). Cavity-filling mutagenesis was applied to every hydrophobic and aromatic residue present in gp140 (362 mutants), introducing amino acids with side chains of a larger size than the native residues (changing A to V, F to Y, V to L, and I/L/S/T/N/Q to F). The mutants were all introduced into a parental version of the B41 SOSIP.664 construct that contained a C-terminal D7324 epitope tag to facilitate screening by ELISA. Taken together, the three mutagenesis strategies yielded 852 mutants (Table 1).

To identify variants with improved antigenicity, each B41 SOSIP.664 mutant protein was expressed in human cells and screened against PGT151, PG9, and PGT145 bNAbs in a capture ELISA format (Fig. 2). Briefly, the constructs were transiently expressed in human HEK-293T cells for 48 h in a 384-well format, each well containing a different

TABLE 1 Mutagenesis libraries created for B41 SOSIP.664 trimer engineering[a]

Mutagenesis strategy	No. of variants in library	No. of variants expressed[b]	No. of hits identified in primary screen[c]	No. of hits identified in secondary screen[d]
Dicysteine scan	341	275	41	7
Cavity fill	362	298	38	10
Proline scan	149	146	30	12
All strategies	852	719	109	29

[a]The libraries of mutants used in this study comprise 852 sequence-confirmed gp140 variants.
[b]Based on the binding of any of the MAbs PG9, PGT145, PGT151, and b6 being ≥70% of the parental binding.
[c]Based primarily on PGT151 binding (more than 2 standard deviations above background).
[d]Based on PGT151 or PG9 binding (significantly higher than parental binding [$P < 0.05$, Student's t test]).

variant. The culture supernatants were then transferred to a 384-well ELISA plate coated with the D7324 epitope tag capture antibody. Each well was then probed with PGT151, PG9, or PGT145. In addition, the nonneutralizing MAb b6 served as a probe for the total production level of Env (trimeric and nontrimeric); a substantial increase in b6 binding (relative to that of other MAbs) can also be indicative of damaging mutations that compromise trimer formation. The binding of each test MAb in all three libraries was normalized to their binding to the parental B41 SOSIP.664 construct. Among the 852 mutants, 719 were expressed at levels that allowed further analysis, based on their reactivity with at least one of the MAbs at ≥70% of the signals derived from the parental B41 SOSIP.664 construct (Table 1). The reactivity profile of all four MAbs with each of these 719 mutants was next used to select clones for additional secondary screening. Because of the poor reactivity of PGT151 with the parental construct, the key criterion for antigenicity improvement was a PGT151 binding signal at least 2 standard deviations greater than that for the parental B41 SOSIP.664 trimer. In total, 109 of the 719 expressed mutants were selected for secondary screening.

We found that PGT145 was the most sensitive probe for structural perturbations irrespective of the mutagenesis method, based on its decreased reactivity (625 of 852 mutants across the libraries) (Fig. 3). The sensitivity of PGT145 binding is consistent with its known absolute specificity for native-like trimers (21, 22). Of the three individual mutagenesis strategies, the introduction of cysteine pairs was the most detrimental to trimer antigenicity. Nearly all of the cysteine pair variants (99%, 338 of 341) resulted in decreased PGT145 binding. Conversely, the cavity-filling strategy was the least detrimental, as only 47% of these variants (170 of 362) resulted in decreased PGT145 binding.

The 109 antigenically improved variants identified in the primary screen were subjected to a secondary screen that retested each of them in quadruplicate and now also included MAb PG16 and soluble CD4 (sCD4) as additional probes of antigenic integrity. Hits in the secondary screen were defined primarily by a PGT151 binding signal that was significantly greater ($P < 0.05$) than that obtained with the parental construct. In total, 29 variants met this benchmark (Table 2). The reactivities of the other MAb probes were also considered, but their reactivity profiles were generally indicators of impaired rather than improved antigenicity. Nevertheless, it was notable that three of the selected mutants (Q203F, T538F, and I548F) were more reactive with PG9 and PGT151. Because of the unbiased nature of the mutagenesis strategies across the $gp41_{ECTO}$ or gp140 sequence, nearly all of the mutations identified are novel. However, some are close to or similar to mutations that have been identified previously and are being pursued in other studies (1, 10, 12).

Visualizing mutations on the trimer structure. The 29 variants (containing 30 different residues) identified in the secondary screen were visualized on the JR-FL SOSIP.664 trimer structure (PDB identifier 5FUU), with the goal of understanding how they might be improving the presentation of the PGT151 epitope (Fig. 4). More specifically, we sought to assess whether these sequence changes affected the global antigenicity of the trimer and its overall presentation of various conformation-sensitive

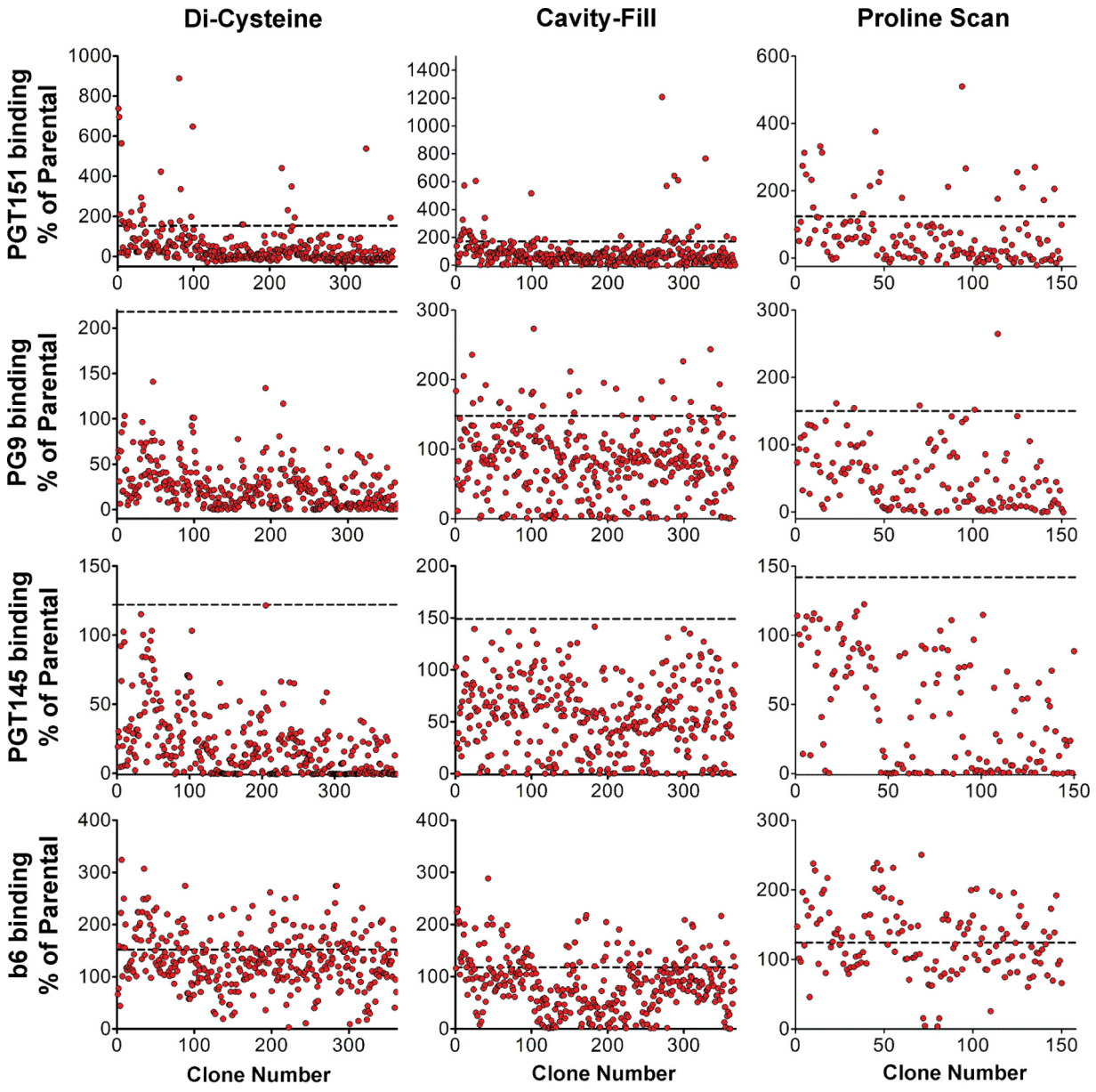

FIG 2 Screens of three mutagenesis libraries to identify B41 SOSIP.664 gp140 variants with increased bNAb binding. The scatterplots show the distribution of binding by the MAbs indicated on the left in one experiment that is representative of duplicate screens. The three types of libraries created are indicated at the top. The horizontal dashed line in each graph indicates 2 standard deviations above the value for the parental B41 SOSIP.664 gp140 (parental reactivity defined as 100%). Because PGT151 binds so poorly to the parental B41 gp140, some of the increases in binding for reactive mutants are proportionately much greater than for the other test MAbs.

bNAb epitopes. The mutants include four that increased PGT151 ELISA binding by >10-fold, i.e., the Q203F, T538F, I548F, and M629P mutants (Fig. 5A). T538F, I548F, and M629P are located in gp41 (Fig. 5B), while Q203F is located in gp120. The Q203F mutation in the C2 region of gp120 caused 11-fold and 2-fold increases in PGT151 and PGT145 binding, respectively. For I548F, the increases in PGT151 and PGT145 binding were 13-fold and 3-fold, respectively. The M629P mutation, which is located in HR2 just N-terminally to a turn in the helix, increased PGT151 binding by 11-fold and PGT145 binding by 2-fold. The increases in PGT145 reactivity induced by each of these mutations are of particular note given that the parental B41 SOSIP.664 trimer already binds PGT145 strongly.

Mutation T538F resulted in an 11-fold increase in PGT151 binding and a 2-fold increase in PG9 binding. Residue T538 lies in gp41 helix α-6 and contacts helix α-9 of

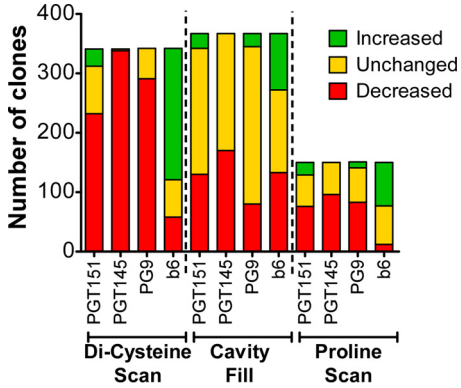

FIG 3 Distribution of primary screening data for MAb binding to B41 gp140 mutagenesis libraries. For each library, data distributions are shown for the changes in binding to MAbs PGT151, PGT145, PG9, and b6 by using the combined data from duplicate primary screens. For the purposes of this graph, we define an antibody signal of 2 standard deviations over the parental signal as an increase, any signal 2 standard deviations below the parental signal as a decrease, and anything less than 2 standard deviations from the parental signal as unchanged. Increases in the reactivity of MAb b6 are indicative of damaging mutations that compromise trimer formation or of increases in total gp140 levels, unlike the other (trimer-sensitive) MAbs.

an adjacent monomer only when PGT151 is bound between the two monomers (Fig. 5C). We hypothesized that replacing threonine with the larger phenylalanine moiety produced more extensive contacts between gp41 monomers and thereby stabilized the trimer structure. To further study residue 538, we substituted all 19 natural amino acids for the wild-type threonine at this position. We then measured PGT151 and PG9 binding to the resulting variant trimers and found that every amino acid that increased reactivity with these bNAbs (e.g., tyrosine, tryptophan, isoleucine) had a large hydrophobic side chain similar to that of phenylalanine (Table 3). However, no residue was better at increasing PGT151 binding than the initially identified phenylalanine substitution. Overall, the data suggest that the T538F mutation stabilizes the B41 SOSIP.664 trimer by filling an otherwise low-density space within the gp41 subunits.

Combinations of mutations that increase PGT151 binding. Residues T538, I548, and M629 are widely separated from one another in gp41 (>17 Å apart), while Q203 is in gp120, separated by >40 Å from the other three mutations. It seemed possible, therefore, that the various mutations may result in independent structural changes with the potential for synergy if they were combined. To test this idea, we made 11 variants representing every possible combination of the Q203F, T538F, I548F, and M629P substitutions and then tested them by capture ELISA using the same test antibodies as in the earlier screens. The outcome was that the T538F Q203F and T538F M629P double mutants, the T538F Q203F I548F and T538F Q203F M629P triple mutants, and the T538F Q203F I548F M629P quadruple mutant were all modestly more reactive with PGT151. However, only for the T538F M629P double mutant was the increase significant compared to the T538F single mutant ($P < 0.05$) (Table 4). Thus, either Q203F or M629P can be beneficially combined with T538F, increasing PGT151 binding by 40% and 57%, respectively. This effect was restricted to PGT151, in that there was no increase in PG9 binding. Combining Q203F with M629P did not increase PGT151 binding further, suggesting that these two sequence changes may either have similar individual effects or be incompatible with one another.

Antigenic characterization of selected mutants. To further characterize the antigenicity of variant B41 trimers, we assembled a panel of 14 MAbs that included bNAbs against multiple different epitope clusters (2G12, VRC01, PG9, PG16, PGT145, PGT151, 35O22, ACS202, 8ANC195, 3BNC60, 3BC315) (see Table 5 for epitope regions). Also included were the non-NAbs b6 to a CD4bs epitope, 17b to a CD4-induced epitope, and 19b to a V3 epitope.

For these studies, we used surface plasmon resonance (SPR) to assess the antigenicity of bNAb and non-NAb epitopes more accurately than is possible by ELISA (7, 22).

TABLE 2 Mutations that result in improved PGT151 antigenicity

Mutation[a]	Domain	% binding (SD)[b]						Conservation (%)[c]
		PGT151	PG	PG16	PGT145	b6	sCD4	
H72C, Q552C†	gp41/120	899 (±140)*	30 (±6)	24 (±8)	0 (±1)	70 (±31)	33 (±2)	97, 99
A73C, L555C†	gp41/120	989 (±95)*	51 (±10)	31 (±10)	101 (±19)	564 (±141)*	33 (±11)	99, 99
H72C, L556C†	gp41/120	293 (±35)*	45 (±14)	31 (±6)	44 (±16)	334 (±75)	19 (±12)	97, 99
A73C, A558C†	gp41/120	375 (±51)*	63 (±17)	59 (±15)	55 (±5)	189 (±8)	16 (±7)	99, 99
V75C, L556C†	gp41/120	266 (±26)*	63 (±19)	48 (±10)	31 (±1)	138 (±24)	34 (±10)	99, 99
A73C, Q562C†	gp41/120	849 (±97)*	58 (±24)	53 (±23)	10 (±5)	346 (±62)*	20 (±4)	99, 99
T77C, Q562C†	gp41/120	296 (±24)*	39 (±11)	30 (±14)	5 (±1)	68 (±10)	41 (±10)	99, 99
L86F	gp120	627 (±50)*	51 (±7)	53 (±24)	98 (±7)	117 (±9)	105 (±17)	91
L111F†	gp120	449 (±39)*	79 (±9)	53 (±12)	80 (±14)	236 (±48)	104 (±33)	98
Q203F	gp120	1,145 (±90)*	117 (±25)	109 (±29)	218 (±11)	67 (±10)	33 (±10)	99
A526V	gp41	244 (±16)*	56 (±13)	228 (±48)	34 (±4)	64 (±15)	73 (±23)	99
T529F	gp41	499 (±56)*	41 (±10)	61 (±15)	26 (±2)	64 (±3)	29 (±8)	99
T538F	gp41	1,110 (±60)*	224 (±30)*	40 (±23)	122 (±9)	33 (±7)	51 (±16)	99
I548F†	gp41	1,342 (±61)*	115 (±19)	50 (±19)	289 (±30)*	116 (±16)	36 (±8)	99
T569F†	gp41	397 (±16)*	55 (±7)	43 (±9)	10 (±2)	50 (±7)	84 (±36)	99
I573F†	gp41	655 (±83)*	62 (±20)	10 (±7)	242 (±30)	94 (±15)	61 (±20)	99
Q577F†	gp41	679 (±114)*	23 (±14)	28 (±11)	76 (±6)	23 (±5)	36 (±11)	98
G516P	gp41	521 (±75)*	35 (±10)	12 (±5)	6 (±1)	196 (±25)	41 (±20)	99
L523P	gp41	230 (±19)*	63 (±25)	46 (±17)	88 (±9)	224 (±33)	68 (±21)	99
G527P	gp41	803 (±52)*	57 (±14)	25 (±6)	76 (±15)	233 (±74)	81 (±18)	99
Q575P†	gp41	567 (±40)*	40 (±6)	9 (±4)	48 (±5)	325 (±28)*	106 (±10)	99
Q577P†	gp41	449 (±38)*	32 (±11)	10 (±4)	4 (±2)	510 (±36)*	79 (±33)	99
A578P†	gp41	605 (±31)*	34 (±6)	17 (±7)	12 (±3)	339 (±36)*	104 (±43)	85
K601P	gp41	622 (±85)*	32 (±8)	63 (±24)	45 (±10)	684 (±128)*	172 (±31)*	96
T618P	gp41	345 (±48)*	64 (±11)	35 (±12)	174 (±31)	91 (±10)	98 (±35)	16
L619P	gp41	351 (±34)*	60 (±14)	38 (±9)	96 (±7)	108 (±10)	77 (±21)	34
D624P	gp41	277 (±30)*	41 (±12)	62 (±10)	53 (±6)	193 (±2)	57 (±7)	43
M629P	gp41	1,142 (±71)*	62 (±12)	64 (±10)	190 (±18)	285 (±67)	98 (±17)	72
K633P	gp41	225 (±6)*	44 (±12)	36 (±13)	41 (±3)	330 (±27)*	66 (±36)	36

[a]All mutations are numbered using the HXB2 convention. The Q203F, T538F, I548F, and M629P mutations that are studied further here are underlined. A dagger denotes a residue that is in the PGT151 binding footprint (20).

[b]Secondary screen data for the most PGT151-reactive variants, recorded as the percentage binding of each MAb relative to the parental construct, with standard deviations in parentheses. Due to the low baseline binding to the parental construct, increases in PGT151 binding to the variants can be very large in percentage terms. *, significantly higher than the wild-type value ($P < 0.05$, Student's t test).

[c]Conservation indicates how conserved the indicated residue(s) is among all HIV-1 Env isolates (http://www.hiv.lanl.gov).

The four B41 Q203F, T538F, I548F, and M629P single mutants, as well as the Q203F T538F I548F triple mutant, were all compared with the parental B41 SOSIP.664 trimer. All trimers were purified by 2G12 affinity chromatography, followed by size exclusion chromatography (SEC), with all mutants resulting in approximately equivalent yields (~0.5 mg/liter). Trimers were then captured onto Biacore CM5 chips using a D7324 antibody directed to their C-terminal epitope tags. The various MAbs were then injected as solution-phase analytes (7, 22).

Of the single mutations, T538F conferred the most favorable antigenic changes, increasing PGT151 and PGT145 binding while decreasing that of the non-NAb 19b. The Q203F and I548F mutations also both increased PGT151 binding, but they had differential binding effects on the apical quaternary epitopes (the profiles shown in Fig. 6 are quantified below [see Table 5]).

The effects on the CD4bs epitopes also differed among the single mutants. Q203F increased the binding of the bNAb 3BNC60 and reduced that of the non-NAb b6. V3 exposure on the mutants also varied: whereas T538F and Q203F reduced the binding of the non-NAb 19b, I548F increased it. The M629P mutation was associated with some favorable antigenic improvements but also increased the binding of both b6 and 19b, a combination of unfavorable antigenic effects not seen with the other mutant trimers.

The variously favorable mutations were combined into a triple mutant (the Q203F T538F I548F mutant), which demonstrated both more extreme improvements and impairments in its antigenic profile. Thus, PGT151 bound 5-fold better to the triple mutant than to the parental trimer, while the binding of the nonneutralizing MAbs b6 and 19b was eliminated. However, these beneficial changes were accompanied by the

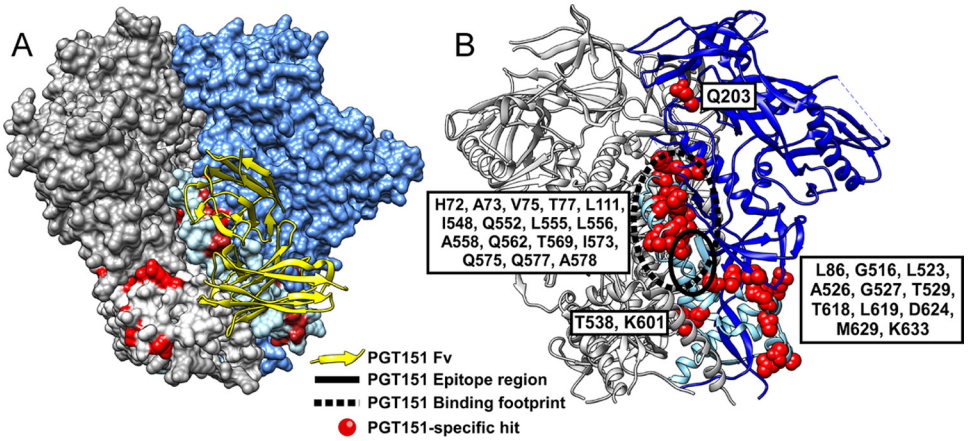

FIG 4 Location of mutations that increase PGT151 binding to B41 SOSIP.664 trimers. (A) The 29 mutants identified in the screening assays that increase PGT151 binding involve 30 different amino acids; the seven dicysteine mutants involve nine different amino acids, and Q577 was changed to both a Phe and a Pro (Table 2). (B) The same mutations as shown in panel A are mapped on one protomer of a gp140 ribbon structure to allow better visualization of internal residues. Amino acids are highlighted in red on the JR-FLΔCT cryo-EM structure (PDB identifier 5FUU), showing those that lie within or very close to the PGT151 binding footprint as defined by lower-resolution negative-stain electron microscopy (oval enclosed by dashed lines) (20) or that make direct contact (<4.2 Å) with PGT151 as defined by higher-resolution cryo-EM (oval enclosed by solid line) (27). Other mutated residues are more distantly located.

reduced binding to other gp120-gp41 interface MAbs (35O22, ACS202, and 8ANC195) and to a gp41 epitope MAb (3BC315). Finally, the triple mutant bound the CD4bs bNAb VRC01 more weakly but a second CD4bs bNAb, 3BNC60, more strongly than the parental trimer did. The latter observation is noteworthy since 3BNC60 is the more broadly active and potent of these two CD4bs bNAbs (23).

Overall, our data suggest that increased PGT151 reactivity is possible, in many cases accompanied by other antigenicity improvements, but may sometimes come at the cost of reduced antigenicity for other bNAb epitopes (discussed below).

Thermostability and visualization of B41 trimer variants. To measure whether the mutations introduced into B41 SOSIP.664 had any effect on trimer stability and integrity, we performed differential scanning calorimetry (DSC) and negative-stain electron microscopy (EM) analyses of 2G12- and SEC-purified trimers. The largest gains in melting temperature (thermal denaturation midpoint [T_m]) were seen with the T538F and I548F mutants (+0.9°C and +4.4°C, respectively) (Fig. 7A and B). This increase in thermostability is consistent with our initial speculation that introducing a larger aromatic residue may increase the strength of interactions between gp41 regions, adding to the overall stability of the trimer.

All the B41 SOSIP.664 variants resembled the parental trimers in that they formed fully native-like trimers when examined by EM (Fig. 7C). Moreover, all the variants exhibited greater flexibility at the 3-fold symmetric axis (75 to 100% open native conformation) than the parental B41 trimers (40% open native) or BG505 trimers (which primarily exist in the closed native conformation) (6). Since BG505 binds well to PGT151, this partially open phenotype does not, therefore, appear to influence the ability of a trimer to bind PGT151 (or, for that matter, impact thermal stability). Rather, the mutations appear to be affecting the equilibrium between more compact and more open native states (i.e., trimer "breathing"), although the molecular mechanisms and antigenic consequences of such changes are still under investigation. The EM analysis also showed that all the B41 trimer variants retained their structural integrity, with no visible indication of monomers, dimers, or nonnative trimers.

DISCUSSION

A long-term goal of the HIV-1 vaccine field has been the development of a soluble envelope gp140 trimer (i.e., one containing the ectodomains but not the transmem-

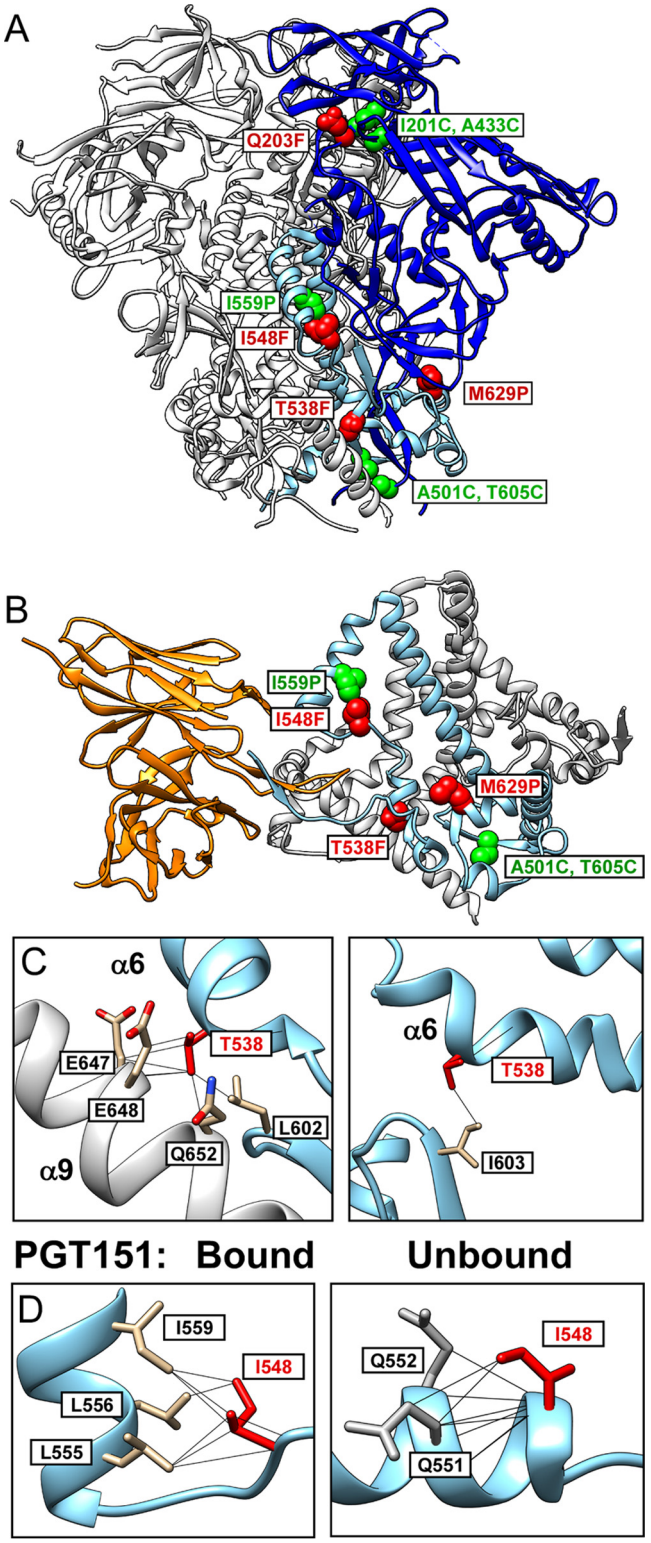

FIG 5 Mutations that stabilize the PGT151 epitope. (A) The sites of the mutations that best increased PGT151 binding (Q203F, T538F, I548F, M629P) are shown in red on the JR-FL trimer structure (PDB identifier 5FUU). Shown in green for comparative purposes are the locations of amino acids commonly mutated in engineered trimers, such as the I559P mutation that maintains SOSIP trimers in their prefusion conformation, the SOS disulfide bond involving A501C and T605C, and an additional engineered disulfide bond involving I201C and A433C that locks gp140 in the prefusion conformation. The gp120 subunits are represented by dark blue ribbons, gp41 by light blue. (B) The sites of the T538F, I548F, and M629P mutations are shown on the gp41 trimer bound to PGT151 (orange) (PDB identifier 5FUU).

(Continued on next page)

TABLE 3 Saturation mutagenesis of residue T538[a]

	% binding (SD)	
T538 substitution[b]	**PGT151**	**PG9**
Alanine	90 (±11)	111 (±10)
Arginine	43 (±3)	131 (±13)
Asparagine	80 (±2)	93 (±4)
Aspartate	34 (±2)	77 (±6)
Cysteine	56 (±3)	52 (±6)
Glutamine	45 (±3)	106 (±2)
Glutamate	40 (±2)	115 (±7)
Glycine	75 (±7)	81 (±2)
Histidine	109 (±10)	111 (±7)
Isoleucine	402 (±14)*	137 (±10)
Leucine	39 (±3)	105 (±9)
Lysine	29 (±1)	108 (±19)
Methionine	213 (±15)*	137 (±4)
Phenylalanine	588 (±51)*	111 (±10)
Proline	39 (±2)	45 (±4)
Serine	81 (±5)	111 (±10)
Threonine (WT)	100 (±9)	100 (±7)
Tryptophan	510 (±14)*	129 (±8)
Tyrosine	469 (±8)*	134 (±6)
Valine	274 (±10)*	117 (±11)

[a]B41 SOSIP.664 mutants containing 19 different amino acid substitutions of residue T538 were tested for PGT151 binding by capture ELISA. The results are presented as the % binding (with standard deviation) of the mutant with the indicated substitution relative to that of the wild type (WT) with a threonine residue (defined as 100%). *, significant increase in signal compared to that of the WT (T538) (Student's *t* test, $P < 0.05$).

[b]The substitution in the T538F mutant that is studied further here is underlined.

brane or cytoplasmic domains) that mimics the native structure and antigenicity of virion-associated gp160 (2, 24). Trimers with appropriate properties have now been developed, allowing high-resolution cryo-EM and X-ray structures to be obtained and preclinical immunogenicity data to be generated (2, 11). The SOSIP.664 construct has been the most widely studied native-like soluble trimer. Here we sought to understand why the SOSIP.664 trimer based on the clade B strain B41 does not mimic the full antigenic properties of B41 virion-associated gp160 and to identify trimers with improved antigenicity. Accordingly, we used both informed (rational) design elements and empirical (high-throughput) screening elements to engineer improved trimer variants.

One of the primary screening criteria for our studies was the restoration of the PGT151 bNAb epitope at the gp120-gp41 interface. That epitope was unexpectedly absent from B41 SOSIP.664 trimers but is present on their BG505 counterparts. We also included other bNAbs in the screen, particularly ones against trimer apex epitopes that, like the PGT151 site, are highly sensitive to trimer conformation. In addition, we sought to minimize the exposure of non-NAb epitopes that may serve as immunological distractions. Individual mutations could influence MAb epitopes either directly (due to modifications of binding contacts) or indirectly (by affecting the global structure of the trimer in a way that stabilizes distantly located bNAb epitopes). Such mutations could also have broader applicability to trimer structure and stability. Ultimately, our screening criteria were guided by selection criteria both positively (increased binding to PGT151 and increased or unaffected binding to PGT145 and PG9) and negatively (decreased or unaffected binding to b6 and sCD4).

FIG 5 Legend (Continued)
The Q203F substitution located in gp120 is not shown. (C) The location of T538 is shown in the context of gp41 helices α-6 and α-9 on a PGT151-bound (left) and -unbound (right) face of the trimer. Residue 648 is glutamate in JR-FL (shown) and valine in B41, residue 602 is leucine in JR-FL and isoleucine in B41, residue 559 is an isoleucine in both JR-FL and B41 but is changed to a proline in SOSIP trimers, and the other contact residues shown are identical between JR-FL and B41. (D) The location of I548 is shown in the context of local interactions on a PGT151-bound (left) and -unbound (right) face of the trimer.

TABLE 4 Combinations of mutations that increase PGT151 binding[a]

Mutation(s)	% binding (SD)[b]				
	PGT151	PG9	PGT145	b6	sCD4
T538F	100 (±11)	100 (±17)	100 (±28)	100 (±9)	100 (±14)
Q203F	35 (±17)†	50 (±13)†	81 (±19)	103 (±9)	91 (±13)
I548F	30 (±6)†	59 (±10)†	113 (±7)	204 (±17)*	100 (±11)
M629P	41 (±23)†	64 (±10)†	59 (±6)†	329 (±55)*	184 (±18)*
T538F, Q203F	157 (±52)	111 (±19)	107 (±15)	51 (±3)†	127 (±20)
T538F, I548F	66 (±9)†	50 (±8)†	101 (±8)	52 (±8)†	38 (±5)†
T538F, M629P	140 (±20)*	90 (±11)	90 (±12)	158 (±24)*	99 (±15)
Q203F, I548F	38 (±4)†	54 (±16)†	96 (±15)	73 (±4)†	51 (±13)†
Q203F, M629P	35 (±6)†	55 (±17)†	86 (±27)	91 (±34)	78 (±62)
I548F, M629P	28 (±11)†	29 (±4)†	60 (±10)	213 (±19)*	98 (±11)
T538F, Q203F, I548F	129 (±45)	98 (±16)	124 (±13)	30 (±6)†	30 (±4)†
T538F, Q203F, M629P	137 (±57)	55 (±5)†	73 (±13)	67 (±13)†	105 (±14)
T538F, I548F, M629P	79 (±17)	48 (±1)†	75 (±5)	77 (±10)†	48 (±4)†
Q203F, I548F, M629P	39 (±11)†	35 (±8)†	77 (±10)	122 (±2)*	75 (±8)†
T538F, Q203F, I548F, M629P	117 (±16)	68 (±11)†	130 (±7)	49 (±6)†	37 (±3)†
Parental B41	30 (±21)†	37 (±12)†	69 (±13)	245 (±46)*	137 (±20)*

[a]The four mutations to the parental B41 SOSIP.664 construct that gave the greatest increase in PGT151 binding were introduced in all possible combinations, and the mutants were screened by capture ELISA.

[b]The results for the binding of each MAb are presented as % binding (with standard deviation) relative to that of the T538F single mutant (defined as 100%). Significant increases (*) and significant decreases (†) in binding relative to that of the T538F single mutant (Student's *t* test, $P < 0.05$) are indicated.

The types of mutagenesis strategies used here are based on approaches that have been successful in other trimer engineering projects but that here were systematically applied throughout the B41 gp140 construct. Dicysteine scanning to introduce new disulfide bonds has been used to lock gp120 to gp41 in defined conformations (8, 24). Helix-destabilizing proline substitutions have previously been used to improve the stability of soluble trimers by introducing the side chain into a position where the helical conformation would be disfavored (25). Space-filling mutations can stabilize trimers by occupying internal cavities with larger amino acid side chains that form additional hydrophobic packing contacts with neighboring residues (12, 15). Each of these strategies resulted in improved B41 trimer variants that could be identified in our screens (Tables 1 and 2) but also disrupted trimer production and/or integrity in many cases. For example, dicysteine scanning resulted in the largest proportion of variants (291 of 341, 85%) with decreased reactivity with key bNAbs in the primary screen (Fig. 3). Overall, cavity-filling mutations proved to be the most productive strategy, resulting in the three best individual mutants we identified (the Q203F, T538F, and I548F mutants).

The antigenic effects of the studied mutations were varied (Table 5). Some mutations increased the reactivity of certain bNAbs but decreased that of others. For example, the T538F mutant overall had the most beneficial antigenic changes, with increased binding of bNAbs PGT151 and PGT145 and decreased binding of the non-NAb 19b. Other bNAbs were relatively unaffected by T538F, including 35O22 and ACS202, that also bind the gp120-gp41 interface, but 8ANC195 reactivity was reduced. A similar but more extreme pattern of both favorable and unfavorable changes in antigenicity was seen with the Q203F T538F I548F triple mutant; it bound PGT151 markedly better, but its reactivity with the gp120-gp41 interface bNAbs 35O22, ACS202, and 8ANC195 was impaired. Such opposed antigenic effects likely reflect underlying structural changes (e.g., around the fusion peptide) that stabilize some bNAb interactions while destabilizing others (26). The increased PGT151 reactivity therefore appears to come at the cost of reduced antigenicity for other bNAb epitopes. Hence, protein engineering strategies can be useful for improving specific bNAb epitopes but may have limitations when the goal is a more comprehensive improvement to antigenicity. Such factors may need to be taken into account when designing trimers for inducing germ line bNAb responses to specific epitopes. Conversely, protein engineering methods that target individual epitopes within larger clusters could be beneficial for

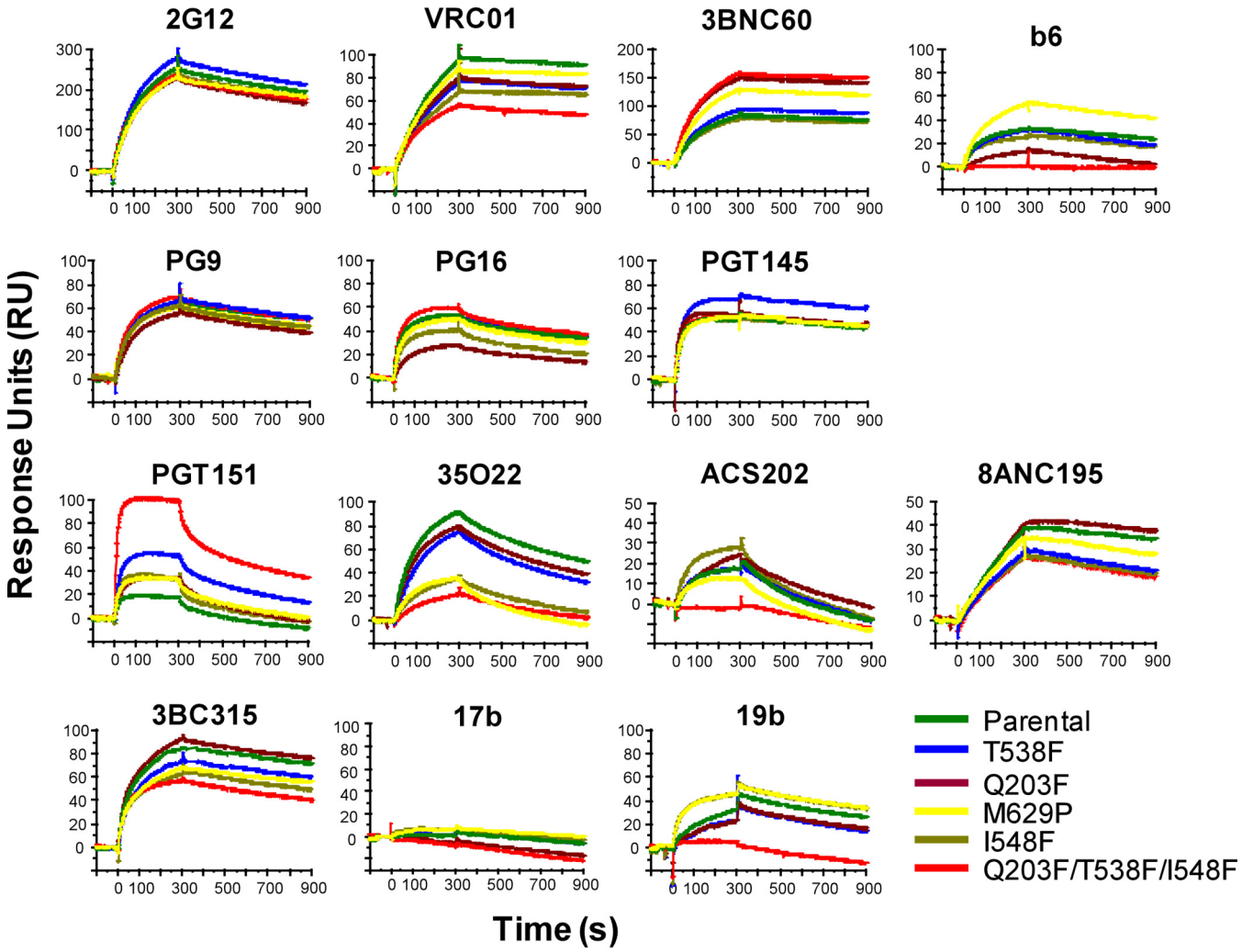

FIG 6 Antigenic characterization of select mutants by SPR. Each sensorgram graph shows the binding of one MAb to different B41 SOSIP.664 variants. Binding was monitored for 300 s of association and 600 s of dissociation. The signal in response units on the *y* axis is proportional to the mass of bound MAb. The *y* axis scales are adjusted based on the extent of MAb binding and hence are not the same on every panel. Results are quantified in Table 5.

immunofocusing strategies. While the B41 SOSIP.664 trimer variants identified here are fully native-like by DSC and EM, their immunogenicity has yet to be tested. We also have yet to explore whether the mutations identified here have systematically or more narrowly beneficial effects on trimers based on other HIV-1 strains.

Two of the most beneficial mutations, T538F and I548F, involve phenylalanine substitutions within the somewhat flexible HR1 helix of gp41. The T538F mutation is proximal to a hydrophobic pocket at the base of the trimer, where HR1 and HR2 are tightly packed (Fig. 5C). Thus, the introduction here of phenylalanine (or other aromatic residues [Table 3]) likely provides additional stability and locks the N-terminal HR1 region into this pocket. Of note is that the overall structure of this region remains the same in the unbound and PGT151-bound states of the trimer. In contrast, the HR1 region where the I548 mutation is located undergoes a conformational change upon PGT151 binding, as shown in the cryo-EM model of PGT151-bound, membrane-extracted JR-FL Env (27) (Fig. 5D). In each conformation, I548 is buried in a different hydrophobic pocket. In the PGT151-bound state, the side chain of I548 is in close proximity to the side chains of I559 and F53. The soluble SOSIP.664 trimers retain their prefusion conformation in large part due to the I559P mutation that prevents springing of the HR1 helix (25). In this context, the I548F mutation may allow the formation of stabilizing interactions with F53 and possibly I/P559 and I555.

A Summary of DSC and EM analysis

Sample	Tm (°C)	ΔTM (°C)	%Native EM
Parental (-R315Q)	58.3	-1.1	100
Parental	59.4	0	100
T538F	60.3	+0.9	100
I548F	63.8	+4.4	100
Q203F	58.3	-1.1	100
M629P	57.9	-1.5	100

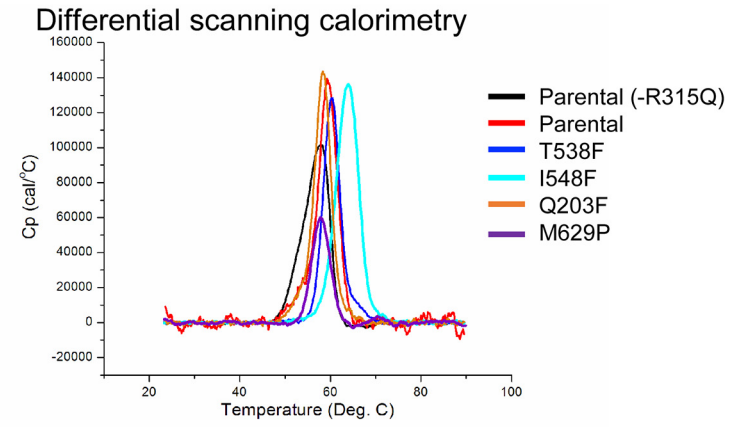

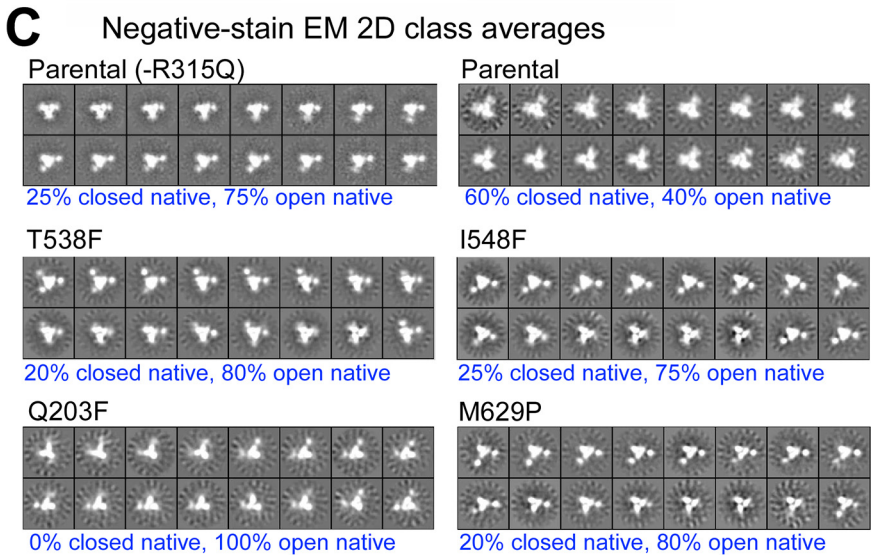

FIG 7 Biophysical characterization of B41 SOSIP.664 mutants. (A) Summary of differential scanning calorimetry and negative-stain EM (NS-EM) data. T_m, thermal denaturation point; ΔT_m, difference in T_m from parental B41 SOSIP.664 trimers; % Native, percentage of particles that resemble native-like trimers. Increases in T_m are relative to that of the parental B41 SOSIP.664 trimer used in this study, which contains an R315Q point mutation in V3 that was included in all mutants to decrease proteolytic clipping. The R315Q change itself confers a small (1.1°C) increase in thermostability over that of the same B41 trimer without the R315Q change. (B) Overlay of normalized DSC curves reveal differences in T_m values between the trimer variants. Reported T_m values are for the highest peak of each sample. Cp, heat capacity. (C) NS-EM two-dimensional class averages of trimer variants. The estimates of the percentages of particles classified as having closed native-like and open native-like features were based on methods described previously (12).

Overall, our results suggest that mutations such as T538F can improve the antigenic and stability profile of SOSIP.664. The strategies used here to obtain improved trimer variants may also be useful for improving other properties that are desirable for a commercial vaccine, such as easier manufacturing scale-up (yield), simpler immunogen

TABLE 5 Antigenic characterization of select mutants[a]

mAb	Epitope Region	Neut/ Non-neut	Parental	Q203F	T538F	I548F	M629P	Q203F T538F I548F
2G12	Mannose, V3-base	Neut	250-254	229-230	278-279	230-240	220-230	235-250
VRC01	CD4-binding site	Neut	90-95	79-80	76	64-67	84-87	55-61
3BNC60	CD4-binding site	Neut	82-83	148-150	86-93	78-80	128-129	144-158
b6	CD4-binding site	Non-neut	33	14-15	30-31	25-26	54-55	1.0-5.0
PG9	Apex	Neut	65-82	55-62	66-88	62-65	62-72	60-69
PG16	Apex	Neut	54-55	29-31	52-64	41-48	50	55-60
PGT145	Apex	Neut	50-51	50-54	60-68	50	52-53	48-53
PGT151	gp120-gp41 interface	Neut	18	34-36	54-61	34-42	33	90-99
35O22	gp120-gp41 interface	Neut	92	80-85	75-87	35-39	36	22-24
ACS202	gp120-gp41 interface	Neut	17-18	24-25	18-22	28-31	13	-1.0-2.0
8ANC195	gp120-gp41 interface	Neut	38	40-41	28-29	26-27	34-35	22-26
3BC315	gp41 intersubunit	Neut	85-88	93-97	73-74	50-63	68-69	54-57
17b	CD4-induced	Non-neut	1.0-2.0	-5.8-5.0	2.5-3.7	5.9-6.8	6.2-6.6	-6.8-7.9
19b	V3	Non-neut	33-35	23-26	23-24	46-51	46-48	5.4-6.8

[a]MAb binding to B41 SOSIP.664 variants was measured by SPR. Response values shown (in RU) are measured at the end (300 s) of the association phase and represent the ranges for two replicates. Gray shading indicates an increase in binding relative to the parental binding (>125%), and pink shading indicates a decrease in binding relative to the parental binding (<75%). 17b, which recognizes an epitope induced by CD4, did not detectably bind to any trimer. Neut, neutralizing; Non-neut, nonneutralizing.

storage (temperature stability), and longer shelf life (retention of antigenic properties over time). Selection for additional antigenic properties is also of course possible. The high-throughput mutagenesis and systematic screening approaches we have described here provide a basis for identifying additional variants that meet these challenges.

MATERIALS AND METHODS

High-throughput scanning mutagenesis. A shotgun mutagenesis mutation library was created for B41 SOSIP.664 gp140 (formally 9032-08_A1.4685; GenBank accession no. EU576114), as previously described (28, 29). Briefly, plasmid B41 SOSIP.664-D7324 Env was used as a parental template with one additional mutation (R315Q) in the V3 region that changes GPGR to GPGQ to eliminate V3 proteolytic clipping during production (30). Based on previously successful strategies for engineering trimers, we prepared three libraries to systematically apply these strategies across gp140: dicysteine mutations at predicted stabilization sites throughout gp140, a proline scan at every residue of $gp41_{ECTO}$, and a cavity-filling scan across the entire gp140 molecule. For the dicysteine scan, selected residues were mutated to Cys together with other residues predicted to be possible S-S bond partners. Residue selections for dicysteine scanning (in HXB2 numbering) were as follows: amino acids 72 to 80 against amino acids 550 to 570, 162 to 164 against 309 to 313, 198 to 201 against 431 to 435, 527 to 531 against 623 to 629, 535 to 539 against 648 to 656, 662 to 664 against 499 to 504, and V36C, Y40C, W45C, P493C, G495C, A497C, P498C, T499C, A501C against each of D589C, W596C, T605C, V608C, P609C, and W610C. For the cavity-filling scan, hydrophobic and aromatic residues were replaced with a larger residue as follows: A to V, F to Y, V to L, and I, L, S, T, N, or Q to F. In total, 852 gp140 mutants were generated, sequence confirmed, and arrayed into 384-well plates. Variants that failed mutagenesis or sequencing were not included in further studies. Each well of the mutation array plate contained one defined mutant, and each plate included eight positive-control (parental B41 SOSIP.664) and four negative-control (pUC19) wells. Each mutant was transfected individually into human HEK-293T cells along with a furin expression plasmid at a 4:1 ratio. The cells were incubated for 48 h in Dulbecco's modified Eagle medium (DMEM; Thermo Scientific, Waltham, MA) containing 10% fetal bovine serum (FBS) before cell supernatants were collected and transferred to wells of a D7324 capture ELISA plate for screening.

ELISA screening of gp140 transfection supernatants. Primary screening for stabilized trimers was carried out by a capture ELISA. Nunc 384-well high-binding MaxiSorp plates were coated overnight with 10 μg/ml of sheep polyclonal antibody D7324 (Aalto Bio Reagents, Dublin, Ireland) diluted in 0.1 M sodium carbonate-sodium bicarbonate buffer, pH 9.6. The D7324 antibody recognizes an epitope tag present on the C terminus of each gp140 protein. The plates were then washed three times with phosphate-buffered saline without calcium or magnesium ($PBS^{-/-}$) and blocked for 1 h in 3% bovine serum albumin (BSA; Sigma-Aldrich, St. Louis, MO) prepared in $PBS^{-/-}$. Blocking buffer was removed, and trimers were added to each well. The volume of supernatant (i.e., amount of gp140 protein) added for

each ELISA was optimized for each detection antibody, and the total volume of each well was increased to 20 μl by adding complete DMEM. The plates were incubated for 2 h at room temperature, with shaking, and then washed three times with $PBS^{-/-}$ before the addition of the primary antibody at the following optimized concentrations: PGT151, 2 μg/ml; PGT145, 0.5 μg/ml; PG9, 1 μg/ml; PG16, 0.5 μg/ml; b6, 0.5 μg/ml; and sCD4-Fc (human IgG Fc fusion), 0.25 μg/ml. After a further 1 h of incubation, the plates were washed three times with $PBS^{-/-}$, and the secondary antibody (Novex goat anti-human IgG–horseradish peroxidase [HRP] conjugate) was added for 30 min. Finally, the plates were washed three times with $PBS^{-/-}$, and 20 μl of SuperSignal West Pico chemiluminescent HRP substrate was added per the manufacturer's protocol (Thermo Fisher Scientific). The luminescence signal was quantified 1 min after substrate addition using a Perkin-Elmer Envision plate reader.

Cellular immunofluorescence detection of gp160. HIV-1 gp160 expression constructs were transfected into HEK-293T cells in a 384-well plate, and the cells were cultured for 22 h. The immunoreactivity of each MAb, over a range of concentrations, was determined by reactivity with unfixed cells. The cells were incubated with each MAb diluted in 10% normal goat serum (NGS; Sigma-Aldrich, St. Louis, MO) and then incubated with each anti-Env MAb for 1 h at room temperature, washed twice with $PBS^{-/-}$, and incubated for a further 30 min with Alexa Fluor 488-conjugated secondary antibody (Jackson ImmunoResearch Laboratories, West Grove, PA) in 10% NGS. After the cells were washed twice with $PBS^{-/-}$, they were resuspended in Cellstripper (Cellgro, Manassas, VA) plus 0.1% BSA. Cellular fluorescence was detected using a high-throughput flow cytometer (Intellicyt, Albuquerque, NM). The background fluorescence signal was determined using empty vector-transfected control cells, and this value was subtracted from signals derived using Env-transfected cells.

Infectivity and neutralization assays. Reporter viruses pseudotyped with HIV-1 Env were produced essentially as described previously (31) by cotransfecting a gp160 plasmid with plasmids encoding HIV-1 core proteins (Gag-pol) and luciferase (pNL-luc, based on pNL4-3-R^-E^-). The transfected cells were incubated for 48 to 72 h at 37°C in 5% CO_2 for pseudovirus production. The supernatants were harvested and stored at −80°C. Target HEK-293T cells were transfected with plasmids to express CD4 and CCR5 in a 96-well white plate at 0.4×10^6 cells/well in DMEM containing 10% FBS and incubated at 37°C in 5% CO_2 overnight. The following day, serial dilutions of MAbs were made in DMEM with 10% FBS and 8% DEAE-dextran hydrochloride (Sigma). The test antibodies and pseudotyped viruses were mixed together for 45 min at room temperature and then added to the CD4- and CCR5-transfected HEK-293T cells using a spinoculation procedure in which the infection plates were centrifuged at 2,000 rpm for 1 h at 20°C (Sorvall Legend XTR with swinging-bucket rotor model 75003180). The infected cells were then incubated at 37°C for 24 h before 70 μl of fresh medium was added to each well. Finally, the cells were lysed at 72 h postinfection, and the lysates were assayed for luciferase activity (Promega, Madison, WI).

SOSIP trimer expression and purification. HEK-293F cells were seeded at a density of 5.5×10^4/ml, grown to a density of 1 million cells/ml over 3 days in Corning Hyperflasks, and transfected using 293Fectin (Life Technologies). Briefly, 400 μg of Env-expressing plasmid and 100 μg of furin-expressing plasmid were mixed with 1 ml of 293Fectin in Opti-MEM medium and added to 250 ml of growth medium. The final concentrations of the gp140 and furin plasmids in serum-free medium were 0.53 μg/ml and 0.13 μg/ml, respectively. The supernatant was harvested after 72 h and passed through a 2G12 column made with CNBr-activated Sepharose 4B resin (GE Healthcare) at a flow rate of 1 ml/min, as previously described (6, 14, 32). The beads were washed with 2 column volumes of buffer (20 mM Tris-HCl, 500 mM NaCl, pH 8), and the Env protein was eluted with 1 column volume of 3 M $MgCl_2$ (pH 7.2). The eluted protein was immediately buffer-exchanged into 10 mM Tris-HCl–75 mM NaCl, pH 8, and concentrated using SnakeSkin dialysis tubing (10,000 molecular weight cutoff; Thermo Scientific). The buffer-exchanged proteins were further concentrated using Vivaspin columns with a 30-kDa cutoff (GE Healthcare). Trimer fractions were then isolated by SEC using a Superdex 200 16/600 column (GE Healthcare) and the same buffer. The SEC fractions were analyzed on 4-to-16% Bis-Tris BN-PAGE gels (Invitrogen). The electrophoresis was done at 200 eV for 1 h in native-PAGE running buffer. After Coomassie blue staining, pure trimer fractions were identified and pooled. Protein concentrations were determined using a bicinchoninic acid-based assay (BCA assay; Thermo Scientific). The protein was stored at −80°C. The purity of trimer in the final stock was estimated from the blue native gel to be >95%.

Antigenic characterization assays using SPR. Surface plasmon resonance (SPR) assays were carried out as described previously (22). Briefly, purified D7324-tagged trimers were captured onto CM5 chips by the covalently bound polyclonal, affinity-purified D7324 antibody (Aalto Bio Reagents, Dublin, Ireland) to ligand immobilization levels (R_L) of 500 response units (RU) (mean, 504 RU; 95% confidence interval, 502 to 505 RU). Each MAb was then injected at 500 nM; association was monitored for 300 s and dissociation for 600 s. A flow rate of 50 μl/min was used throughout in order to minimize mass transport limitations. The signal from a parallel control channel with capture Ab but without trimer was subtracted throughout. After each cycle of MAb binding, the D7324-conjugated surface was regenerated by a single pulse of 10 mM glycine (pH 2.0) for 60 s at a flow rate of 30 μl/min.

Differential scanning calorimetry and electron microscopy. Trimers purified by the 2G12 affinity and SEC method were exchanged into PBS (pH 7.2) using centrifugal filter units (Millipore) and diluted to 0.25 mg/ml. Samples were loaded onto a MicroCal VP-capillary DSC instrument (Malvern) and subjected to a 20-to-90°C ramp at 60°/h. Origin 7.0 software was used to subtract baseline measurements and to fit the melting curves using a non-two-state model. Reported T_m values are for the tallest peak of each sample. Sample preparation, data collection, data processing, and analysis for negative-stain electron microscopy were as described previously (12).

ACKNOWLEDGMENTS

This work was supported by NIH grants R43 AI102626 (B.J.D.), P01 AI110657 (J.P.M., R.W.S., A.B.W., and P.J.K.), and R37 AI36082 (J.P.M. and P.J.K.).

We thank David Tucker, Joseph Rucker, Silveria Rodriguez, Christine Rettew, and Albert Cupo for valuable technical assistance and scientific advice. We thank the International AIDS Vaccine Initiative (IAVI) for providing valuable MAb reagents for this project.

J.T.S., C.S, and B.J.D. are employees of Integral Molecular. B.J.D. is a shareholder of Integral Molecular. Integral Molecular offers protein engineering services on a commercial basis. The commercial affiliation of these authors does not alter their adherence to journal policies on sharing data and materials. The other authors have no relevant conflicts of interest.

REFERENCES

1. de Taeye SW, Moore JP, Sanders RW. 2016. HIV-1 envelope trimer design and immunization strategies to induce broadly neutralizing antibodies. Trends Immunol 37:221–232. https://doi.org/10.1016/j.it.2016.01.007.
2. Sanders RW, Moore JP. 2017. Native-like Env trimers as a platform for HIV-1 vaccine design. Immunol Rev 275:161–182. https://doi.org/10.1111/imr.12481.
3. Khayat R, Lee JH, Julien JP, Cupo A, Klasse PJ, Sanders RW, Moore JP, Wilson IA, Ward AB. 2013. Structural characterization of cleaved, soluble HIV-1 envelope glycoprotein trimers. J Virol 87:9865–9872. https://doi.org/10.1128/JVI.01222-13.
4. Iyer SP, Franti M, Krauchuk AA, Fisch DN, Ouattara AA, Roux KH, Krawiec L, Dey AK, Beddows S, Maddon PJ, Moore JP, Olson WC. 2007. Purified, proteolytically mature HIV type 1 SOSIP gp140 envelope trimers. AIDS Res Hum Retroviruses 23:817–828. https://doi.org/10.1089/aid.2006.0261.
5. Julien JP, Lee JH, Ozorowski G, Hua Y, Torrents de la Pena A, de Taeye SW, Nieusma T, Cupo A, Yasmeen A, Golabek M, Pugach P, Klasse PJ, Moore JP, Sanders RW, Ward AB, Wilson IA. 2015. Design and structure of two HIV-1 clade C SOSIP.664 trimers that increase the arsenal of native-like Env immunogens. Proc Natl Acad Sci U S A 112:11947–11952. https://doi.org/10.1073/pnas.1507793112.
6. Pugach P, Ozorowski G, Cupo A, Ringe R, Yasmeen A, de Val N, Derking R, Kim HJ, Korzun J, Golabek M, de Los Reyes K, Ketas TJ, Julien JP, Burton DR, Wilson IA, Sanders RW, Klasse PJ, Ward AB, Moore JP. 2015. A native-like SOSIP.664 trimer based on an HIV-1 subtype B *env* gene. J Virol 89:3380–3395. https://doi.org/10.1128/JVI.03473-14.
7. Sanders RW, Derking R, Cupo A, Julien JP, Yasmeen A, de Val N, Kim HJ, Blattner C, de la Pena AT, Korzun J, Golabek M, de Los Reyes K, Ketas TJ, van Gils MJ, King CR, Wilson IA, Ward AB, Klasse PJ, Moore JP. 2013. A next-generation cleaved, soluble HIV-1 Env trimer, BG505 SOSIP.664 gp140, expresses multiple epitopes for broadly neutralizing but not non-neutralizing antibodies. PLoS Pathog 9:e1003618. https://doi.org/10.1371/journal.ppat.1003618.
8. Garces F, Lee JH, de Val N, de la Pena AT, Kong L, Puchades C, Hua Y, Stanfield RL, Burton DR, Moore JP, Sanders RW, Ward AB, Wilson IA. 2015. Affinity maturation of a potent family of HIV antibodies is primarily focused on accommodating or avoiding glycans. Immunity 43:1053–1063. https://doi.org/10.1016/j.immuni.2015.11.007.
9. Julien JP, Cupo A, Sok D, Stanfield RL, Lyumkis D, Deller MC, Klasse PJ, Burton DR, Sanders RW, Moore JP, Ward AB, Wilson IA. 2013. Crystal structure of a soluble cleaved HIV-1 envelope trimer. Science 342:1477–1483. https://doi.org/10.1126/science.1245625.
10. Kwon YD, Pancera M, Acharya P, Georgiev IS, Crooks ET, Gorman J, Joyce MG, Guttman M, Ma X, Narpala S, Soto C, Terry DS, Yang Y, Zhou T, Ahlsen G, Bailer RT, Chambers M, Chuang GY, Doria-Rose NA, Druz A, Hallen MA, Harned A, Kirys T, Louder MK, O'Dell S, Ofek G, Osawa K, Prabhakaran M, Sastry M, Stewart-Jones GB, Stuckey J, Thomas PV, Tittley T, Williams C, Zhang B, Zhao H, Zhou Z, Donald BR, Lee LK, Zolla-Pazner S, Baxa U, Schon A, Freire E, Shapiro L, Lee KK, Arthos J, Munro JB, Blanchard SC, Mothes W, Binley JM, McDermott AB, Mascola JR, Kwong PD. 2015. Crystal structure, conformational fixation and entry-related interactions of mature ligand-free HIV-1 Env. Nat Struct Mol Biol 22:522–531. https://doi.org/10.1038/nsmb.3051.
11. Ward AB, Wilson IA. 2017. The HIV-1 envelope glycoprotein structure: nailing down a moving target. Immunol Rev 275:21–32. https://doi.org/10.1111/imr.12507.
12. de Taeye SW, Ozorowski G, Torrents de la Pena A, Guttman M, Julien JP, van den Kerkhof TL, Burger JA, Pritchard LK, Pugach P, Yasmeen A, Crampton J, Hu J, Bontjer I, Torres JL, Arendt H, DeStefano J, Koff WC, Schuitemaker H, Eggink D, Berkhout B, Dean H, LaBranche C, Crotty S, Crispin M, Montefiori DC, Klasse PJ, Lee KK, Moore JP, Wilson IA, Ward AB, Sanders RW. 2015. Immunogenicity of stabilized HIV-1 envelope trimers with reduced exposure of non-neutralizing epitopes. Cell 163:1702–1715. https://doi.org/10.1016/j.cell.2015.11.056.
13. Klasse PJ, LaBranche CC, Ketas TJ, Ozorowski G, Cupo A, Pugach P, Ringe RP, Golabek M, van Gils MJ, Guttman M, Lee KK, Wilson IA, Butera ST, Ward AB, Montefiori DC, Sanders RW, Moore JP. 2016. Sequential and simultaneous immunization of rabbits with HIV-1 envelope glycoprotein SOSIP.664 trimers from clades A, B and C. PLoS Pathog 12:e1005864. https://doi.org/10.1371/journal.ppat.1005864.
14. Sanders RW, van Gils MJ, Derking R, Sok D, Ketas TJ, Burger JA, Ozorowski G, Cupo A, Simonich C, Goo L, Arendt H, Kim HJ, Lee JH, Pugach P, Williams M, Debnath G, Moldt B, van Breemen MJ, Isik G, Medina-Ramirez M, Back JW, Koff WC, Julien JP, Rakasz EG, Seaman MS, Guttman M, Lee KK, Klasse PJ, LaBranche C, Schief WR, Wilson IA, Overbaugh J, Burton DR, Ward AB, Montefiori DC, Dean H, Moore JP. 2015. HIV-1 neutralizing antibodies induced by native-like envelope trimers. Science 349:aac4223. https://doi.org/10.1126/science.aac4223.
15. Chuang GY, Geng H, Pancera M, Xu K, Cheng C, Acharya P, Chambers M, Druz A, Tsybovsky Y, Wanninger TG, Yang Y, Doria-Rose NA, Georgiev IS, Gorman J, Joyce MG, O'Dell S, Zhou T, McDermott AB, Mascola JR, Kwong PD. 2017. Structure-based design of a soluble prefusion-closed HIV-1-Env trimer with reduced CD4 affinity and improved immunogenicity. J Virol https://doi.org/10.1128/JVI.02268-16.
16. Guenaga J, Dubrovskaya V, de Val N, Sharma SK, Carrette B, Ward AB, Wyatt RT. 2015. Structure-guided redesign increases the propensity of HIV Env to generate highly stable soluble trimers. J Virol 90:2806–2817. https://doi.org/10.1128/JVI.02652-15.
17. Kong L, He L, de Val N, Vora N, Morris CD, Azadnia P, Sok D, Zhou B, Burton DR, Ward AB, Wilson IA, Zhu J. 2016. Uncleaved prefusion-optimized gp140 trimers derived from analysis of HIV-1 envelope metastability. Nat Commun 7:12040. https://doi.org/10.1038/ncomms12040.
18. Guenaga J, de Val N, Tran K, Feng Y, Satchwell K, Ward AB, Wyatt RT. 2015. Well-ordered trimeric HIV-1 subtype B and C soluble spike mimetics generated by negative selection display native-like properties. PLoS Pathog 11:e1004570. https://doi.org/10.1371/journal.ppat.1004570.
19. Scharf L, Wang H, Gao H, Chen S, McDowall AW, Bjorkman PJ. 2015. Broadly neutralizing antibody 8ANC195 recognizes closed and open states of HIV-1 Env. Cell 162:1379–1390. https://doi.org/10.1016/j.cell.2015.08.035.
20. Blattner C, Lee JH, Sliepen K, Derking R, Falkowska E, de la Pena AT, Cupo A, Julien JP, van Gils M, Lee PS, Peng W, Paulson JC, Poignard P, Burton DR, Moore JP, Sanders RW, Wilson IA, Ward AB. 2014. Structural delineation of a quaternary, cleavage-dependent epitope at the gp41-gp120 interface on intact HIV-1 Env trimers. Immunity 40:669–680. https://doi.org/10.1016/j.immuni.2014.04.008.
21. Lee JH, Andrabi R, Su C-Y, Yasmeen A, Julien J-P, Kong L, Wu NC, McBride R, Sok D, Pauthner M, Cottrell CA, Nieusma T, Blattner C, Paulson JC,

Klasse PJ, Wilson IA, Burton DR, Ward AB. 2017. A broadly neutralizing antibody targets the dynamic HIV envelope trimer apex via a long, rigidified and anionic β-hairpin structure. Immunity 46:690–702. https://doi.org/10.1016/j.immuni.2017.03.017.
22. Yasmeen A, Ringe R, Derking R, Cupo A, Julien JP, Burton DR, Ward AB, Wilson IA, Sanders RW, Moore JP, Klasse PJ. 2014. Differential binding of neutralizing and non-neutralizing antibodies to native-like soluble HIV-1 Env trimers, uncleaved Env proteins, and monomeric subunits. Retrovirology 11:41. https://doi.org/10.1186/1742-4690-11-41.
23. Scheid JF, Mouquet H, Ueberheide B, Diskin R, Klein F, Oliveira TY, Pietzsch J, Fenyo D, Abadir A, Velinzon K, Hurley A, Myung S, Boulad F, Poignard P, Burton DR, Pereyra F, Ho DD, Walker BD, Seaman MS, Bjorkman PJ, Chait BT, Nussenzweig MC. 2011. Sequence and structural convergence of broad and potent HIV antibodies that mimic CD4 binding. Science 333:1633–1637. https://doi.org/10.1126/science.1207227.
24. Binley JM, Sanders RW, Clas B, Schuelke N, Master A, Guo Y, Kajumo F, Anselma DJ, Maddon PJ, Olson WC, Moore JP. 2000. A recombinant human immunodeficiency virus type 1 envelope glycoprotein complex stabilized by an intermolecular disulfide bond between the gp120 and gp41 subunits is an antigenic mimic of the trimeric virion-associated structure. J Virol 74:627–643. https://doi.org/10.1128/JVI.74.2.627-643.2000.
25. Sanders RW, Vesanen M, Schuelke N, Master A, Schiffner L, Kalyanaraman R, Paluch M, Berkhout B, Maddon PJ, Olson WC, Lu M, Moore JP. 2002. Stabilization of the soluble, cleaved, trimeric form of the envelope glycoprotein complex of human immunodeficiency virus type 1. J Virol 76:8875–8889. https://doi.org/10.1128/JVI.76.17.8875-8889.2002.
26. Lyumkis D, Julien JP, de Val N, Cupo A, Potter CS, Klasse PJ, Burton DR, Sanders RW, Moore JP, Carragher B, Wilson IA, Ward AB. 2013. Cryo-EM structure of a fully glycosylated soluble cleaved HIV-1 envelope trimer. Science 342:1484–1490. https://doi.org/10.1126/science.1245627.
27. Lee JH, Ozorowski G, Ward AB. 2016. Cryo-EM structure of a native, fully glycosylated, cleaved HIV-1 envelope trimer. Science 351:1043–1048. https://doi.org/10.1126/science.aad2450.
28. Davidson E, Doranz BJ. 2014. A high-throughput shotgun mutagenesis approach to mapping B-cell antibody epitopes. Immunology 143:13–20. https://doi.org/10.1111/imm.12323.
29. Paes C, Ingalls J, Kampani K, Sulli C, Kakkar E, Murray M, Kotelnikov V, Greene TA, Rucker JB, Doranz BJ. 2009. Atomic-level mapping of antibody epitopes on a GPCR. J Am Chem Soc 131:6952–6954. https://doi.org/10.1021/ja900186n.
30. Clements GJ, Price-Jones MJ, Stephens PE, Sutton C, Schulz TF, Clapham PR, McKeating JA, McClure MO, Thomson S, Marsh M, Kay J, Weiss RA, Moore JP. 1991. The V3 loops of the HIV-1 and HIV-2 surface glycoproteins contain proteolytic cleavage sites: a possible function in viral fusion? AIDS Res Hum Retroviruses 7:3–16.
31. Fong RH, Banik SS, Mattia K, Barnes T, Tucker D, Liss N, Lu K, Selvarajah S, Srinivasan S, Mabila M, Miller A, Muench MO, Michault A, Rucker JB, Paes C, Simmons G, Kahle KM, Doranz BJ. 2014. Exposure of epitope residues on the outer face of the chikungunya virus envelope trimer determines antibody neutralizing efficacy. J Virol 88:14364–14379. https://doi.org/10.1128/JVI.01943-14.
32. Ringe RP, Yasmeen A, Ozorowski G, Go EP, Pritchard LK, Guttman M, Ketas TA, Cottrell CA, Wilson IA, Sanders RW, Cupo A, Crispin M, Lee KK, Desaire H, Ward AB, Klasse PJ, Moore JP. 2015. Influences on the design and purification of soluble, recombinant native-like HIV-1 envelope glycoprotein trimers. J Virol 89:12189–12210. https://doi.org/10.1128/JVI.01768-15.